Microscale Liquid Metal Conductors for Stretchable and Transparent Electronics

Laurent Dejace, Haotian Chen, Ivan Furfaro, Giuseppe Schiavone, and Stéphanie P. Lacour*

Integrated wearable electronics capable of transducing and transmitting biophysical information on complex and dynamic systems are attracting high interest across the consumer electronics, clinical, and research domains. Gallium and gallium-based liquid metals (LMs) emerge as promising conductor technology for wearables due to their excellent combination of electrical conductivity and mechanical compliance. However, LMs feature complex physical and chemical properties that pose significant manufacturability challenges. Herein, a microtechnology approach is presented to fabricate deformable, microscale LM conductors with high surface density and over large surface areas. Based on a combination of soft lithography, directional patterning, and thermal evaporation of gallium, this new technology enables a range of designs and geometries that can be used to form LM-based stretchable electronic conductors. The versatility of the technology enables a palette of circuit designs that can offer unrivaled transparency ($T > 89\%$) or large metallization density (2/5 μm line/gap).

1. Introduction

Wearable devices are revolutionizing numerous fields such as digital health, gaming, and robotics by allowing the extraction of biophysical information from complex and dynamic systems.[1,2] When coupled to the body, e.g., wearable devices may be implemented as electronic systems that collect useful information from external objects or allow interactions with the environment. While conventional electronics are built with rigid, inelastic materials, a challenge in upcoming wearable technologies is to achieve device functionality while ensuring seamless (mechanical) integration with the human skin. In the past decade, various approaches based on miniaturized transducers and circuits integrated in thin elastomeric and adhesive membranes have been proposed,

identifying, in particular, soft conductor technologies.[3,4] Gallium and gallium-based liquid metals (LMs) have attracted considerable attention.[5] Leveraging their near room temperature liquid–solid phase transition ($T = 29.8$ °C) and large electrical conductivity ($>3 \times 10^6$ S m^{-1}), LMs have been used, often embedded in silicone carriers, as stretchable electrical conductors to carry power and information or transducers with multiple functionalities.[5–10] Because of their complex rheology, however, LMs on elastic substrates have not yet been widely employed in reliable, high-performance, miniaturized circuits owing to challenges in developing patterning techniques that are compatible with wafer-based microtechnology.[11] LMs form a thin (≈1–3 nm thick), solid oxide skin at their surface when exposed to air.[12–14] The oxide counterbalances the high surface tension of LMs and allows wetting of most surfaces. This phenomenon is one of the main hindering factors that prevent today large industrial scale integration of LM electronic technology.

Several techniques have been developed to overcome the manufacturability limitations of LM film conductors.[11,15,16] In one approach, LM patterns are formed by rupturing the oxide skin, forming the desired shape and stabilizing it by regrowth of the oxide skin. 3D and transfer printing techniques relying on this oxide skin stabilization were used to demonstrate traces with microscale resolution.[17–20] Such methods, however, have not been proven compatible with large-area (>cm²) circuit fabrication or do not provide a sufficient control on the LM morphology and cannot therefore guarantee high stretchability (>30%). A similar approach based on laser ablation was also demonstrated for the fabrication of scalable and high-resolution LM grids.[21] While laser micromachining enables high-resolution LM conductor tracks down to 4 μm linewidth, this "serial" technique is incompatible with large metallization density patterning. In another approach, the oxide skin growth is either prevented by processing under vacuum or chemically removed to allow wetting of the LM on an adhesion layer to increase the affinity with the substrate. This approach was used to form stretchable (>100% elongation) and narrow (5 μm) patterns by selective plating LMs on a metallic wetting layer.[22] However, high-resolution circuits over large areas are yet to be achieved.

L. Dejace, H. Chen, I. Furfaro, G. Schiavone, S. P. Lacour
Bertarelli Foundation Chair in Neuroprosthetic Technology
Laboratory for Soft Bioelectronic Interfaces
Institute of Microengineering
Institute of Bioengineering
Centre for Neuroprosthetics
Ecole Polytechnique Fédérale de Lausanne
Geneva 1202, Switzerland
E-mail: stephanie.lacour@epfl.ch

The ORCID identification number(s) for the author(s) of this article can be found under https://doi.org/10.1002/admt.202100690.

2. Results and Discussion

We report on a wafer-scale manufacturing approach combining soft lithography, directional patterning of the LM wetting layer,
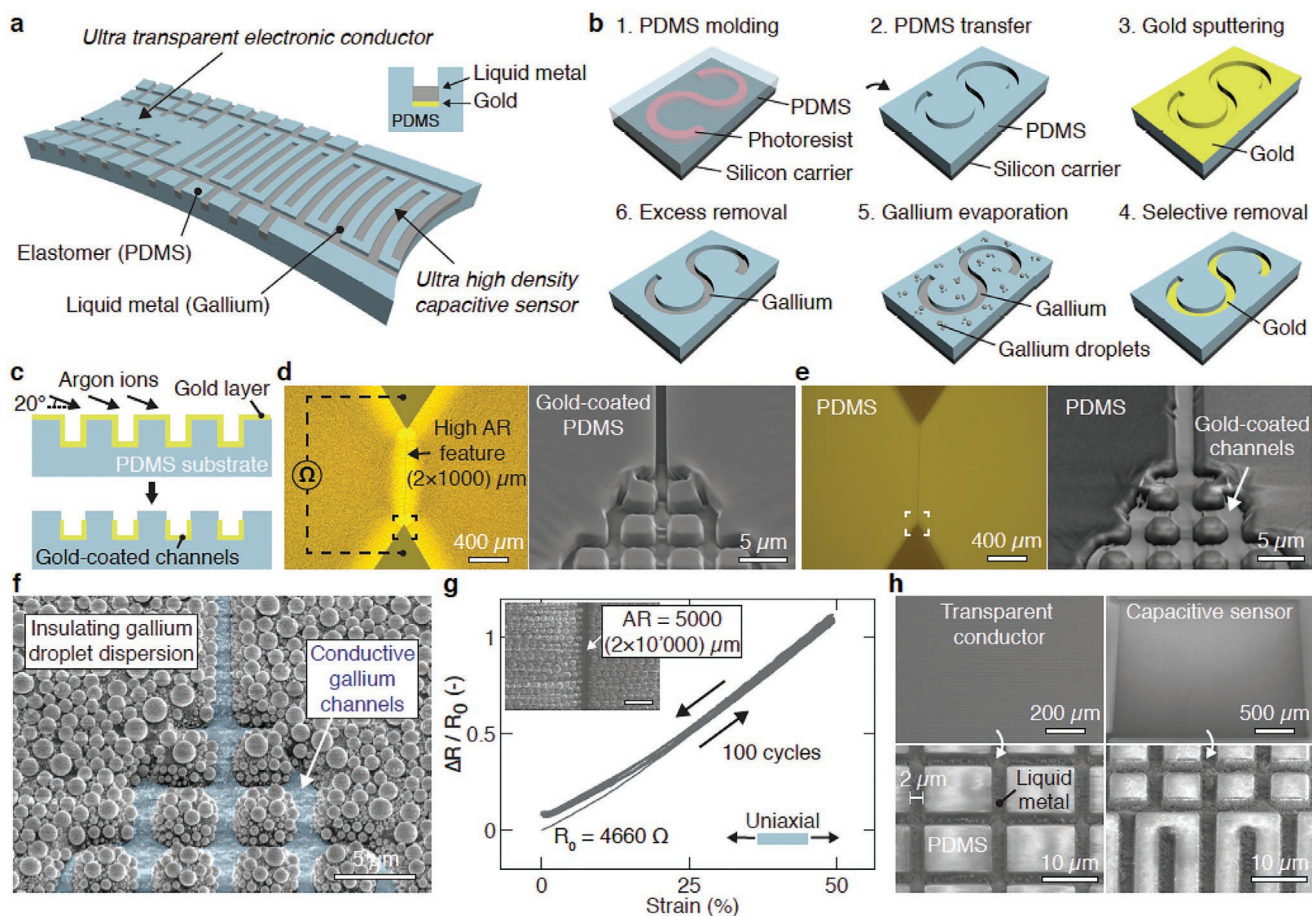
**ADVANCED
SCIENCE NEWS**

www.advancedsciencenews.com

**ADVANCED
MATERIALS
TECHNOLOGIES**

www.advmattechnol.de

Figure 1. High-resolution maskless patterning of LM conductors. a) 3D scheme of high-resolution LM (gallium) patterns on silicone elastomer (PDMS) enabling large-area, ultra-transparent stretchable electronic conductors. Inset: cross-section of the 2×3 µm width x height PDMS microchannels, with an $\approx$80 nm sputtered gold film coating the base surface for the subsequent alloying with thermally evaporated 500 nm LM. b) Manufacturing process. 1) Spin-coating and curing of the PDMS over a soft lithography microchannel mold. 2) Transfer of the PDMS substrate on a new silicone carrier. 3) Gold layer blanket sputtering. 4) Directional gold removal by ion beam etching. 5) LM deposition by thermal evaporation. 6) Removal of the excess LM. c) Optical microscopy (left) and SEM (right) images of a gold-coated, textured PDMS substrate patterned into high aspect ratio (AR) conductors (width: 2 µm, length: 1000 µm). d) Cross-sectional scheme of the gold-coated, textured PDMS substrates before (top) and after (bottom) directional etching of the gold layer from the exposed surface by using a tilted ion beam etching process. e) False color optical microscopy (left) and SEM (right) images of the device in d) after ion beam etching of the gold layer. f) SEM image of a high aspect ratio LM feature after thermal evaporation of gallium. Inside the microchannels, the LM alloys with the gold to form a thin, solid intermetallic phase (AuGa2) covered by liquid phase gallium. On the gold-stripped surfaces, the low affinity of PDMS to gallium causes the metal to condense and form a nonconductive dispersion of drops. g) Relative change in electrical resistance as a function of strain of a high aspect ratio (AR: 5000) LM conductor track. h) SEM images of large-area (left) transparent conductors and (right) ultra-high density capacitive sensors made of 2 µm wide gallium channels confined in PDMS.

and thermal evaporation of the LM that enables microscale resolution patterning, high surface density of LM patterns, and centimeter-scale area coverage. The fine control on the LM microstructure enables a range of geometries that can be used to form transparent LM-based stretchable conductors but also high density, miniaturized capacitive sensors for proximity sensing (**Figure 1**a). The manufacturing process, which is based on the thermal evaporation and condensation of LM into channels of a textured silicone substrate defined by micromolding, is illustrated in Figure 1b and Figure S1 in the Supporting Information. First, a polydimethylsiloxane (PDMS) layer is cast on a photoresist mold lithographically patterned with the desired microchannel geometry. The PDMS layer is then demolded and transferred to another carrier for further processing on the patterned side. A 80 nm thick gold film is blanket-sputtered on the

textured surface, so as to form a lyophilic layer that increases the adhesion of gallium to the silicone substrate. A tilted ion beam etching (IBE) process is then used to selectively remove the gold layer only from the top surface of the patterned mold. Tilting at a 20° horizontal incidence induces a shadowing effect on the recesses, leaving the gold layer deposited on the lateral and bottom surfaces of the channels unaffected by the etching process. The substrate is then exposed to a surface treatment with a self-assembled layer of silane to make the PDMS surface hydrophobic. Thermal evaporation of pure gallium on a gold film promotes alloying between the metals and formation of a thin, solid intermetallic phase ($AuGa_2$) and a liquid gallium phase on top (Figure S2, Supporting Information).[23,24] This is replicated here on the surfaces where the gold is left intact, while on the silanized PDMS surface the LM condenses
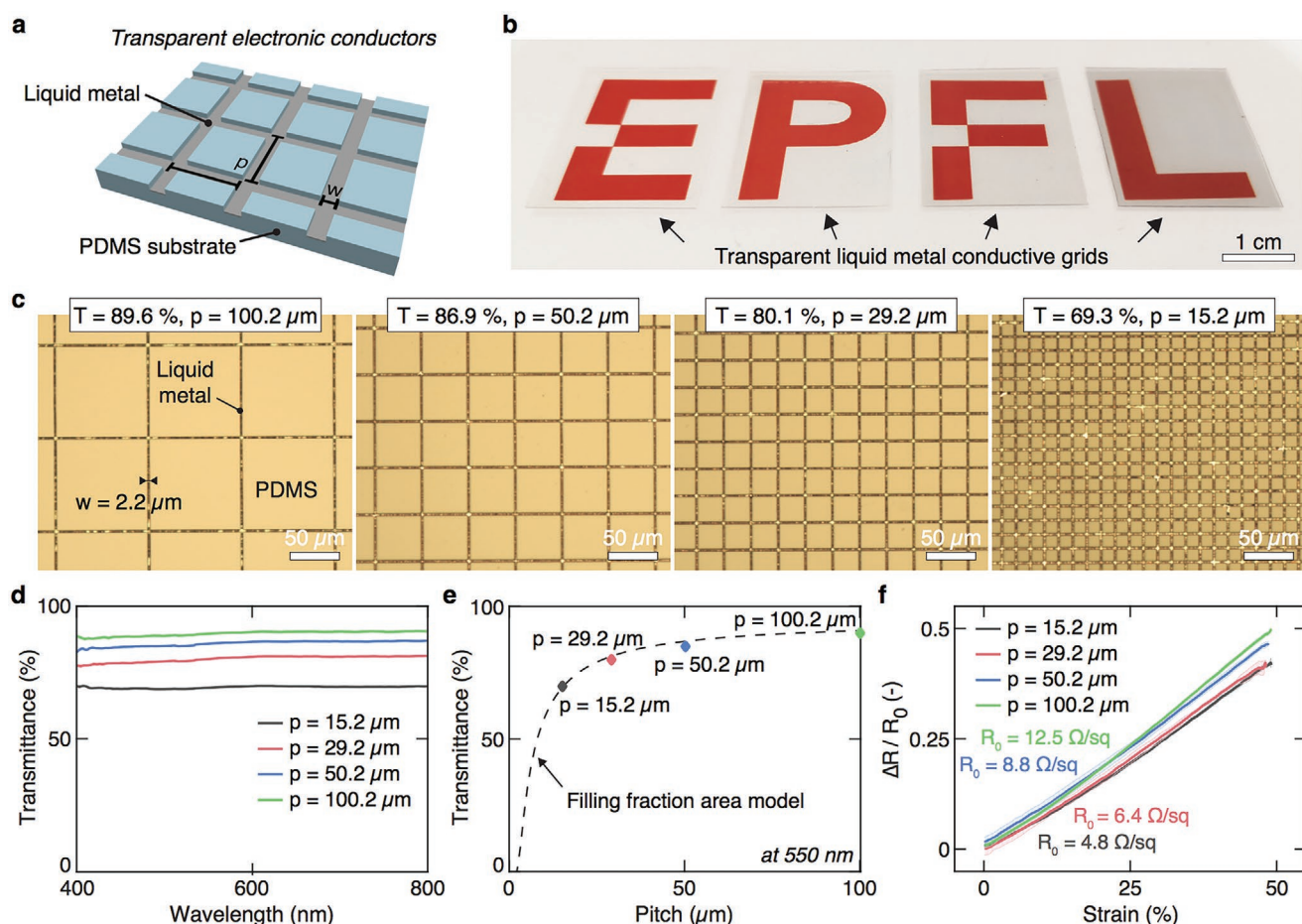
**ADVANCED
SCIENCE NEWS**

www.advancedsciencenews.com

**ADVANCED
MATERIALS
TECHNOLOGIES**

www.advmattechnol.de

Figure 2. Ultra-transparent LM-based electronic conductors. a) 3D scheme of an LM conductor grid (width w = 2.2 μm, pitch p) on PDMS. b) Photographs of transparent LM grids with decreasing transparency from left to right. The grids are overlaid on our university logo to visualize their transparency. c) Optical microscopy images of four LM grids with the same feature width w = 2 μm but variable pitch (p = 100.2, 50.2, 29.2, 15.2 μm) and their corresponding optical transmittance (T = 89.6%, 86.9%, 80.1%, 69.3%), respectively. d) Optical transmittance of four transparent LM grids as a function of incident light wavelengths in the visible range. e) Optical transmittance at 550 nm wavelength of four transparent LM grids for different grid pitch (p = 100.2, 50.2, 29.2, 15.2 μm) and fitting model based on the filling fraction area. f) Relative change in electrical resistance as a function of strain of four gallium transparent LM grids (p = 100.2, 50.2, 29.2, 15.2 μm).

and forms a nonconductive droplet dispersion (Figure S3, Supporting Information). After evaporation, exposition to atmospheric oxygen promotes the formation of the oxide skin that stabilizes the gallium morphology. Next, the carrier is cooled down to −80 °C for 12 h to solidify the gallium. While in this phase, the excess gallium droplet dispersion is removed from the top PDMS surface by stamping (Figure S4, Supporting Information). Finally, the gallium is molten (80 °C for 2 h) to form the liquid phase stretchable conductors.

This new process enables LM patterning with microscale resolution at the wafer-scale (here demonstrated on 4″ carriers). As a demonstrator, a gold-coated textured PDMS substrate was patterned with high length/width aspect ratio (AR > 10000) conductors featuring complex designs and displaying a stable, reversible, and durable electromechanical response to uniaxial mechanical deformation (50% strain) (Figure 1c–g and Figures S5–S9, Supporting Information). By removing the drops from the top PDMS structure, optically clear, high-resolution LM patterns are achieved (Figure 1h).

One of the key advantages of this technology is the ability to manufacture stretchable conductors without trading the achievable resolution at the expense of scalability. Optically clear LM-based devices can be engineered with unprecedented transparency in the visible wavelength range. Such functionality is of high interest for a number of applications including smart displays, contact lenses, or seamless sensors for wearable devices.[25–27] In recent years, different materials and deformation mechanisms, based on percolation networks, buckles, and nanomeshes, have been explored to form stretchable transparent conductors.[27] In general, it is challenging to maximize the electrical conductivity, transparency, and stretchability since these are competing properties. Current limitations also include the inability of most approaches to form transparent conductors with tunable properties over small and/or large surface areas, and deformations allowed only along predefined directions. Here, the high electrical conductivity of gallium and our precise patterning technique are leveraged to form LM conductor grids of linewidth w = 2.2 μm and different pitch (p = 100.2, 50.2,

**ADVANCED
SCIENCE NEWS**
www.advancedsciencenews.com

**ADVANCED
MATERIALS
TECHNOLOGIES**
www.advmattechnol.de

29.2, 15.2 µm) on PDMS substrates (**Figure 2**a and Figure S10, Supporting Information). When superimposed to our university logo, the different opacity of the four structures becomes evident (Figure 2b,c). The spectral dependence in the visible range (400–800 nm wavelength) of the optical transmittance is plotted in Figure 2d. In the relaxed state (no elongation), the LM grids display 550 nm wavelength optical transmittances of 69.3%, 80.1%, 86.9%, and 89.6% for p = 15.2, 29.2, 50.2, and 100.2 µm, respectively (Figure 2e). The most transparent structure therefore displays the highest optical transmittance reported to date for LM conductors.[21] We then compared the optical transmittance of the LM grids to a simple model based on the filling area fraction, which assumes that light is transmitted only through the clear PDMS surface area, with a transparency of 95% (Figure S11, Supporting Information). The optical transmittance of the four structures is in close agreement with the model (R^2 > 0.98), indicating that LM patterns can be tuned in different geometries to balance electrical conductivity and optical transparency. Next, the electrical performance of the grids was evaluated at rest and under mechanical deformation (Figure 2f). At rest, the structures displayed low electrical sheet resistance R_0 = 4.3, 5.4, 7.7, and 10.7 Ω sq^{-1} for p = 15.2, 29.2, 50.2, and 100.2 µm, respectively. These values are comparable with previously reported high conductivity and stretchable transparent conductors.[27] No significant increase in baseline resistance ($\Delta R/R_0$ < 0.2) is observed after mechanical priming (10 cycles at each strain: 10%, 20%, 30%, 40%, and 1 cycle at 50% strain). Furthermore, the structures exhibit a reversible and linear (GF ~ 1, Gauge factor) behavior when mechanically deformed to 50% strain. The accuracy and the robustness of the patterning technique are further demonstrated by stretching the most transparent structure (p = 100.2 µm) to 100% deformation (Figure S12, Supporting Information). The combination of high electrical conductivity (R_0 = 10.7 Ω sq^{-1}), optical transparency (89.6%), and mechanical deformability (100%) ranks our stretchable LM grids among the best-performing transparent conductors reported to date.[27] Comparison maps are provided in Figure S13 in the Supporting Information.

The second key-enabling advantage of our process is the ability to manufacture gallium thin film patterns with micronscale lateral resolution and high surface density over centimeter side surface areas. We demonstrate the potential of this processing capability by fabricating wearable miniaturized capacitive sensors that mechanically comply with the skin and provide unobtrusive motion monitoring.[1,28] The design of such capacitors with an interdigitated, multi-finger periodic structure is presented in **Figure 3**a. The sensor working principle is based on the disturbance of the electric field fringes by an object, which induces a change in capacitance. The versatility of the manufacturing approach is first demonstrated by patterning microscale structures (width H = 2.5 mm, finger length L = 2.5 mm) with variable electrode width w and gap g. Scanning electron microscopy (SEM) images of three well-defined structures (g = 10, 10, 5 µm and w = 2.5, 15, 2.5 µm), hereafter structures 1, 2, and 3 are shown in Figure 3b (Figure S14, Supporting Information). The change in capacitance as a function of the displacement of an object to be detected in proximity was first measured with an automated recording setup (Figure 3c). The baseline capacitances were 7.6, 8.9, and 19.6 pF for

structures 1, 2, and 3, respectively. The density of capacitance of structure 3 (3.14 µF m^{-2}) is comparable with the highest reported to date for LM conductors (Figure S15, Supporting Information).[18] When the object was approached, the capacitance decreased gradually from the baseline value to its minimum and exhibited a reversible behavior. Structure 3 exhibits the highest absolute variation in capacitance and sensitivity (4.3×10^{-4} mm^{-1} from 0 to 10 mm and 1.3×10^{-4} mm^{-1} from 10 to 50 mm), and a trend in agreement ($R^2 \approx 0.95$) with finite element simulations (Figure 3d,e and Figures S16 and S17, Supporting Information). To demonstrate the utility of such miniaturization, an ≈100 µm thick sensor was mounted on the proximal phalanx of the middle finger to measure adduction and abduction movements. The sensors could reliably detect movements performed at different speeds, and the large capacitance changes enabled signal acquisitions without the need for signal processing or electromagnetic shielding layers, two well-known limitations of capacitive sensors.[29] In addition, this conformal and unobtrusive solution is a valid alternative to strain gauges, inertial measurement units, and other standard solutions for finger adduction and abduction monitoring.[30–35]

3. Conclusion

In summary, we presented a manufacturing technique to form stretchable and high-resolution LM features with high surface density coverage and over centimeter side surface areas. The versatility of the pattern design enables the fabrication of high aspect ratio (AR > 10000) features, stretchable transparent conductors (T > 89%), or ultra-dense proximity sensors for stretchable electronic applications. The advances reported in this work highlight the capability and robustness of the microfabrication process and maskless patterning of the wetting layer to form high-resolution LM features (Figure S18, Supporting Information). This key process enables the preparation of substrates for a fully automated LM deposition by thermal evaporation. The wafer-scale, automated process will be key for future scaling up of the production technology with high manufacturing yield.

Future efforts will be devoted toward further increasing the achievable feature resolution by substituting the photolithography mold-patterning step by e-beam lithography and tailoring the process for other substrates in view of applications involving larger mechanical deformations or specific requirements, for instance in the field of soft robotics.

Our work demonstrates promising stretchable transparent conductors and motion monitoring solutions, yet further miniaturization will unlock employment in other fields such as biomedical imaging and photoacoustics,[36] and, more in general, for any application where stretchable, transparent and high-resolution electronics are desirable specifications.

4. Experimental Section

Thin Film Fabrication: A detailed fabrication process is presented in Figure S1 in the Supporting Information. A silicon wafer carrier was treated with an adhesion promoter, bis(trimethylsilyl)amine (HMDS), and spin-coated with a 3 µm thick (2800 rpm, 45 s) layer of photoresist (AZ ECI 3027, AZ Electronic Materials) and baked (1 min, 110 °C). The
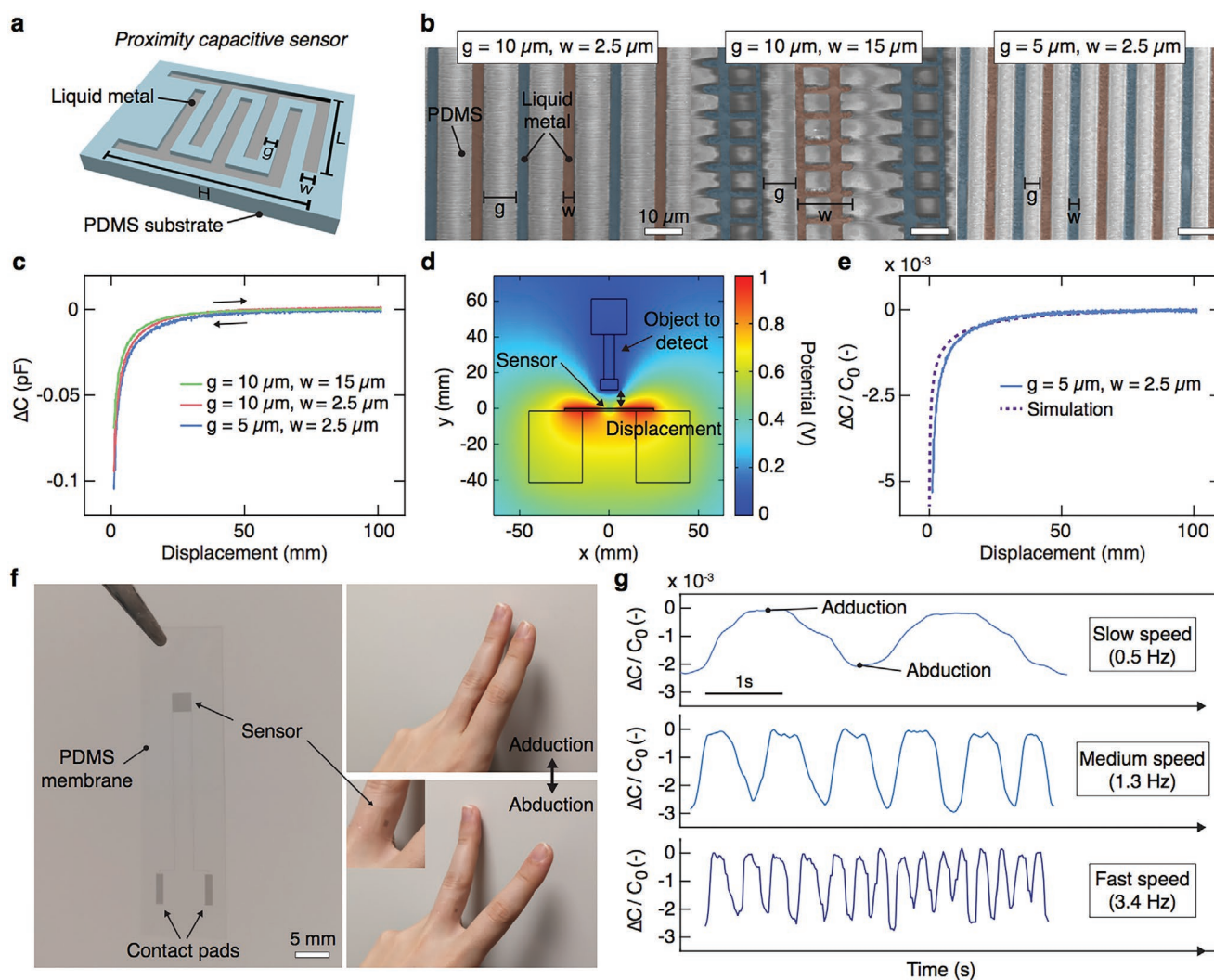
Figure 3. Ultra-high-density capacitive sensors for proximity sensing. a) 3D scheme of an LM capacitive sensor patterned on a PDMS substrate. b) Colored SEM images of three capacitive sensor structures highlighting LM features with different width w and gap g. c) Change in LM sensor capacitance as a function of the displacement of an object to be detected in proximity. In this example, a screw was approached to the sensor from a 100 mm distance to ≈0.3 mm and cycled back to 100 mm at 10 mm s⁻¹. d) Finite element analysis simulation used to compute the electrical potential between the interdigitated sensor electrodes for different screw positions. e) Relative change in capacitance as a function of screw displacement for the sensor with the highest electrode density ($g = 5$ μm, $w = 2.5$ μm) and the numerical analysis curve. f) Photographs of a high density ($g = 5$ μm, $w = 2.5$ μm) capacitive sensor embedded in an ≈100 μm thick PDMS membrane (left) and a sensor mounted on the proximal phalanx of the middle finger to measure adduction and abduction movements (right). g) Relative change of capacitance over time of the proximity sensor during index finger adduction and abduction movements performed at different frequencies.

photoresist was then exposed through a photolithography chromium mask with UV light (355–365 nm) with a dose of 270 mJ cm⁻² (MA6 Gen3, SUSS MicroTech), developed for 90 s in AZ726 MIF (AZ Electronic Materials), and rinsed in deionized (DI) water and dried in air. The photoresist mold was then treated with a self-assembled layer of trichloro(1*h*, 1*h*, 2*h*, 2*h*-perfluorooctyl)silane (Sigma-Aldrich). The textured silicone substrate was formed by preparing PDMS (Sylgard 184, Dow Corning) at a 10:1 ratio of base to curing agent solution by mixing (2 min, 2000 rpm) and defoaming (2 min, 2200 rpm) in a planetary mixer (ARE-250, Thinky), spin-coating (800 rpm, 60 s) as a 60 μm thick film on the photoresist mold, and curing for 2 h at 80 °C. The PDMS was then treated with trichloro(1*h*, 1*h*, 2*h*, 2*h*-perfluorooctyl)silane (Sigma-Aldrich), spin-coated (250 rpm, 1 min) with a 250 μm thick transfer PDMS layer, and cured for 2 h at 80 °C. The two PDMS layers were in turn demolded and transferred upside down to another receiving wafer, which was previously coated with a 60 μm thick (800 rpm, 60 s) liquid

PDMS layer. After planarization (≈10 min), the stack was cured for 2 h at 80 °C. A 80 nm thick gold layer was then blanket sputtered (DP650, Alliance-Concept) on the substrate prior to the directional IBE step, performed at a vertical incidence angle of 70° and during continuous substrate rotation (15 rpm) for ≈7 min. The substrate was then treated with a self-assembled layer of trichloro(1*h*, 1*h*, 2*h*, 2*h*-perfluorooctyl) silane (Sigma-Aldrich) and gallium was thermally evaporated to fill the PDMS substrate textures (E300, Alliance-Concept). The exceeding drops from the top PDMS surfaces were removed by solidifying the gallium films (−80° for 6 h) and transfer printing with a PDMS membrane (60 μm). Small residual gallium particles could further be removed with tape at this stage, while the gallium track inside the channel remained protected. Next, the films were liquefied at (80° for 2 h) to form the stretchable conductors and encapsulated with a PDMS membrane.

High Aspect Ratio Conductors: The high aspect ratio conductors depicted in Figure 1 were prepared using the previously described

**ADVANCED
SCIENCE NEWS**

www.advancedsciencenews.com

**ADVANCED
MATERIALS
TECHNOLOGIES**

www.advmattechnol.de

process, but with a 1.5 µm thick layer of photoresist (instead of 3 µm) to form the silicone textures.

Uniaxial Mechanical Stretching Tests: The PDMS substrates patterned with the metallization were cut, released from the wafer, and clamped in a customized electromechanical setup. The two clamps moved along one axis but in opposite direction to deform the sample at a constant velocity rate (5% s^{-1}). The electrical resistance was measured with a two-point probe setup (2400 source-meter, Keithley) at 6 Hz with a dedicated LabVIEW program.

Transmittance Characterization: The optical properties of the transparent LM grids were studied using transmittance spectroscopy. The transmission spectra of the grids were determined using an integrating sphere (Ocean Optics) between 400 and 800 nm and a spectrometer (USB2000+VIS-NIR-ES, Ocean Optics).

Capacitive Measurements: The capacitance of the interdigitated sensors was measured with an LCR meter (E4980A, Agilent) at 100 kHz and 1 V. The proximity tests were performed with a screw mounted on an Electromechanical Universal Test System (UTS) (C42.503, MTS Systems). The screw approached the sensor from a 100 mm distance to ≈0.3 mm and cycled back to 100 mm at 10 mm s^{-1}.

Supporting Information

Supporting Information is available from the Wiley Online Library or from the author.

Conflict of Interest

The authors declare no conflict of interest.

Data Availability Statement

Research data are not shared.

[1] Y. Ling, T. An, L. W. Yap, B. Zhu, S. Gong, W. Cheng, *Adv. Mater.* **2019**, *32*, 1904664.
[2] J. C. Yang, J. Mun, S. Y. Kwon, S. Park, Z. Bao, S. Park, *Adv. Mater.* **2019**, *31*, 1904765.
[3] M. Amjadi, K. U. Kyung, I. Park, M. Sitti, *Adv. Funct. Mater.* **2016**, *26*, 1678.
[4] T. R. Ray, J. Choi, A. J. Bandodkar, S. Krishnan, P. Gutruf, L. Tian, R. Ghaffari, J. A. Rogers, *Chem. Rev.* **2019**, *119*, 5461.
[5] M. D. Dickey, *Adv. Mater.* **2017**, *29*, 1606425.
[6] K. Khoshmanesh, S. Y. Tang, J. Y. Zhu, S. Schaefer, A. Mitchell, K. Kalantar-Zadeh, M. D. Dickey, *Lab Chip* **2017**, *17*, 974.
[7] C. Wang, C. Wang, Z. Huang, S. Xu, *Adv. Mater.* **2018**, *30*, 1801368.
[8] J. W. Boley, E. L. White, R. K. Kramer, *Adv. Mater.* **2015**, *27*, 2355.
[9] Q. Wang, Y. Yu, J. Yang, J. Liu, *Adv. Mater.* **2015**, *27*, 7109.
[10] S. Chen, H. Z. Wang, R. Q. Zhao, W. Rao, J. Liu, *Matter* **2020**, *2*, 1446.
[11] A. Hirsch, L. Dejace, H. O. Michaud, S. P. Lacour, *Acc. Chem. Res.* **2019**, *52*, 534.
[12] M. D. Dickey, R. C. Chiechi, R. J. Larsen, E. a. Weiss, D.a. Weitz, G. M. Whitesides, *Adv. Funct. Mater.* **2008**, *18*, 1097.
[13] I. D. Joshipura, H. R. Ayers, C. Majidi, M. D. Dickey, *J. Mater. Chem. C* **2015**, *3*, 3834.
[14] J. V. Naidich, J. N. Chuvashov, *J. Mater. Sci.* **1983**, *18*, 2071.
[15] Z. Ma, Q. Huang, Q. Xu, Q. Zhuang, X. Zhao, Y. Yang, H. Qiu, Z. Yang, C. Wang, Y. Chai, Z. Zheng, *Nat. Mater.* **2021**, *20*, 859.
[16] S. Liu, D. S. Shah, R. Kramer-Bottiglio, *Nat. Mater.* **2021**, *20*, 851.
[17] Y.-G. Park, H. S. An, J.-Y. Kim, J.-U. Park, *Sci. Adv.* **2019**, *5*, eaaw2844.
[18] B. A. Gozen, A. Tabatabai, O. B. Ozdoganlar, C. Majidi, *Adv. Mater.* **2014**, *26*, 5211.
[19] M. Kim, H. Alrowais, S. Pavlidis, O. Brand, *Adv. Funct. Mater.* **2017**, *27*, 1604466.
[20] M. Kim, D. K. Brown, O. Brand, *Nat. Commun.* **2020**, *11*, 1002.
[21] C. Pan, K. Kumar, J. Li, E. J. Markvicka, P. R. Herman, C. Majidi, *Adv. Mater.* **2018**, *30*, 1706937.
[22] G. Li, D. W. Lee, *Lab Chip* **2017**, *17*, 3415.
[23] A. Hirsch, H. O. Michaud, A. P. Gerratt, S. de Mulatier, S. P. Lacour, *Adv. Mater.* **2016**, *28*, 4507.
[24] L. Dejace, N. Laubeuf, I. Furfaro, S. P. Lacour, *Adv. Intell. Syst.* **2019**, *1*, 1900079.
[25] T. Q. Trung, N. E. Lee, *J. Mater. Chem. C* **2017**, *5*, 2202.
[26] K. Kim, Y. G. Park, B. G. Hyun, M. Choi, J. U. Park, *Adv. Mater.* **2018**, *31*, 1804690.
[27] Z. H. Chen, R. Fang, W. Li, J. Guan, *Adv. Mater.* **2019**, *31*, 1900756.
[28] Y. Li, S. Nayak, Y. Luo, Y. Liu, H. K. Salila Vijayalal Mohan, J. Pan, Z. Liu, C. H. Heng, A. V.-Y. Thean, *Materials* **2019**, *12*, 1458.
[29] M. L. Hammock, A. Chortos, B. C. K. Tee, J. B. H. Tok, Z. Bao, *Adv. Mater.* **2013**, *25*, 5997.
[30] L. Dipietro, A. M. Sabatini, P. Dario, *IEEE Trans. Syst. Man Cybern. Part C Appl. Rev.* **2008**, *38*, 461.
[31] H. G. Kortier, V. I. Sluiter, D. Roetenberg, P. H. Veltink, *J. Neuroeng. Rehabil.* **2014**, *11*, 70.
[32] Y. Park, J. Lee, J. Bae, *IEEE Trans. Ind. Inf.* **2015**, *11*, 198.
[33] S. Lu, D. Chen, C. Liu, Y. Jiang, M. Wang, *Sens. Actuators, A* **2019**, *285*, 700.
[34] K. Ro, S. Kim, W. Park, J. Bae, *16th Int. Conf. on Control, Automation and Systems (ICCAS)*, IEEE **2016**, p. 549.
[35] L. Wang, T. Meydan, P. I. Williams, *Sensors* **2017**, *17*, 770.
[36] P. Reineck, Y. Lin, B. C. Gibson, M. D. Dickey, A. D. Greentree, I. S. Maksymov, *Sci. Rep.* **2019**, *9*, 5345.